Mamm Genome (2012) 23:404–415
DOI 10.1007/s00335-012-9398-y

Nprl3 is required for normal development of the cardiovascular system

Monika S. Kowalczyk · Jim R. Hughes · Christian Babbs · Luis Sanchez-Pulido · Dorota Szumska · Jacqueline A. Sharpe · Jacqueline A. Sloane-Stanley · Gillian M. Morriss-Kay · Leslie B. Smoot · Amy E. Roberts · Hugh Watkins · Shoumo Bhattacharya · Richard J. Gibbons · Chris P. Ponting · William G. Wood · Douglas R. Higgs

Received: 12 January 2012 / Accepted: 19 March 2012 / Published online: 27 April 2012

Abstract *C16orf35* is a conserved and widely expressed gene lying adjacent to the human *α-globin* cluster in all vertebrate species. In-depth sequence analysis shows that *C16orf35* (now called *NPRL3*) is an orthologue of the yeast gene *Npr3* (nitrogen permease regulator 3) and, furthermore, is a paralogue of its protein partner *Npr2*. The yeast Npr2/3 dimeric protein complex senses amino acid starvation and appropriately adjusts cell metabolism via the TOR pathway. Here we have analysed a mouse model in which expression of *Nprl3* has been abolished using homologous recombination. The predominant effect on RNA expression appears to involve genes that regulate protein synthesis and cell cycle, consistent with perturbation of the mTOR pathway. Embryos homozygous for this mutation die towards the end of gestation with a range of cardiovascular defects, including outflow tract abnormalities and ventriculoseptal defects consistent with previous observations, showing that perturbation of the mTOR pathway may affect development of the myocardium. *NPRL3* is a candidate gene for harbouring mutations in individuals with developmental abnormalities of the cardiovascular system.

Electronic supplementary material The online version of this article (doi:10.1007/s00335-012-9398-y) contains supplementary material, which is available to authorized users.

M. S. Kowalczyk · J. R. Hughes · C. Babbs · J. A. Sharpe · J. A. Sloane-Stanley · R. J. Gibbons · W. G. Wood · D. R. Higgs (✉)
MRC Molecular Haematology Unit, Weatherall Institute of Molecular Medicine, University of Oxford, Oxford OX3 9DS, UK
e-mail: doug.higgs@imm.ox.ac.uk

L. Sanchez-Pulido · C. P. Ponting
MRC Functional Genomics Unit, Department of Physiology, Anatomy and Genetics, University of Oxford, Oxford OX1 3QX, UK

D. Szumska · H. Watkins · S. Bhattacharya
Department of Cardiovascular Medicine and Wellcome Trust Centre for Human Genetics, University of Oxford, Oxford OX3 7BN, UK

G. M. Morriss-Kay
Department of Physiology, Anatomy and Genetics, University of Oxford, Oxford OX1 3QX, UK

L. B. Smoot · A. E. Roberts
Department of Cardiology, Children's Hospital Boston, Boston, MA 02115, USA

Introduction

Of the ~22,000 genes currently annotated in the human genome (GRCh37, 59.37d, Ensembl), the true function is known for only a fraction. Identifying the role played by uncharacterized genes and the proteins they encode is still an important task for fully annotating the functional genome. *C16orf35* is a highly conserved gene that lies upstream of the human *α-globin* cluster in all vertebrates tested (Hughes et al. 2005). Interestingly, this gene contains within its introns three highly conserved regulatory elements (R1–R3) that are required to express the *α-globin* genes at high levels late in erythroid differentiation. Presumably, these embedded regulatory elements have ensured the close linkage (conserved synteny) between *C16orf35* and the *α-globin* genes throughout vertebrate evolution (Hughes et al. 2005). The *C16orf35* gene is widely expressed throughout development, predominantly from a housekeeping promoter that in many species is associated with a classical, unmethylated CpG island. However, we have also noted that expression of the

C16orf35 gene is very highly induced in erythroid cells when the *α-globin* genes are fully activated (Kowalczyk et al. 2012; Lower et al. 2009).

The C16orf35 protein is well conserved across the metazoa with 87, 79, and 36 % amino acid identity of the human protein with its chicken, zebrafish, and *Drosophila* orthologues, respectively (Lunardi et al. 2009). Upon initial inspection, we and others (Lunardi et al. 2009; Neklesa and Davis 2009) could not identify any recognizable sequence features or domains associated with these proteins or any recognizable paralogues. However, more recently others have identified *C16orf35* as a homologue of yeast *Npr3* (nitrogen permease regulator 3). *Npr3* plays a role in sensing amino acid starvation and mediating changes in cellular metabolism via the TOR (target of rapamycin) pathway. Npr3 has been shown to form a dimer with Npr2 (Neklesa and Davis 2009), yet no homology between these subunits has been described. The human protein corresponding to C16orf35 has thus been annotated as NPRL3 (Nitrogen Permease Regulator-Like 3) and it too forms a dimer with NPRL2 (the orthologue of Npr2) in human cells (Neklesa and Davis 2009). This suggests that NPRL2 and NPRL3 form an evolutionarily conserved complex, although its implied role in mTOR (mammalian target of rapamycin) signaling has not been established in human.

To analyse the role of NPRL3 (C16orf35), we analysed in further detail a previously described mouse model in which expression of the Nprl3 protein has been ablated by removal of its constitutive promoter (Kowalczyk et al. 2012). This model has enabled us to examine the effects of a null phenotype in mice in which both alleles have been inactivated. These mice die late in gestation with a range of cardiac defects, including outflow tract abnormalities and ventricular-septal defects.

Materials and methods

Protein sequence alignments

Initial sequence similarity searches were performed with BLAST (Altschul et al. 1997) against the nonredundant protein sequence databases Uniref50 and Uniref90 (Wu et al. 2006). Multiple sequence alignments of homologous protein sequences were generated with the program T-Coffee and HMMer (Eddy 1996; Notredame et al. 2000) using default parameters, slightly refined manually and visualized with the Belvu program (Sonnhammer and Hollich 2005). Profiles of the alignment as global hidden Markov models (HMMs) were generated using HMMer (Eddy 1996). Profile-based sequence searches were performed against Uniref50 (Wu et al. 2006) using HMMsearch (Eddy 1996). Fold recognition analyses were performed using profile-to-profile comparisons with HHpred software (Soding et al. 2005). Secondary structure predictions were acquired using PsiPred (Jones 1999). The NPR2/NPR3 dendrogram in Fig. 1 was generated by the neighbour-joining method (Saitou and Nei 1987) using ClustalW (Higgins et al. 1996) and edited with Treetool (Maciukenas 1994).

More specifically, iterative similarity searches using profile hidden Markov models (HMMer) (Eddy 1996) against the nonredundant protein sequence databases Uniref50 (Wu et al. 2006), with C16orf35 (SwissProt: CP035_HUMAN) N-terminal conserved region (amino acids 66-168) as the query identified remote homologues in the NPR2 family with statistically significant *E* values (inclusion threshold < 0.005). Reciprocally, iterative similarity searches with the NPRL2 (SwissProt: TUSC4_HUMAN) N-terminal conserved region (amino acids 37–124) as the query produced convergent results. Hidden Markov models of the yeast Npr3 domains alignment and those for Npr2 were compared using HHpred (Soding et al. 2005) and found to be highly significant ($E < 10^{-5}$). A protein-domains hunting strategy, based on profile–profile comparisons (HHpred), identified both Npr3 and NPRL2 protein families as having three HTH (helix-turn-helix) domains located at their C termini. Moreover, two high-performing methods of protein structure prediction (Zhang 2008), HHpred and I-TASSER (Soding et al. 2005; Zhang 2008), independently yielded consistent results.

Fetal liver cell culture

Erythroid cells were grown from foetal livers following a published protocol (Dolznig et al. 2001).

RNA sequencing

Total RNA was prepared using Trizol reagent (Sigma) and was *DnaseI*-treated (Ambion). Poly(A)$^+$ mRNA was isolated from total RNA using the PolyA selection kit (Promega) according to the manufacturer's protocol. Poly(A)$^+$ mRNA from erythroid cells was depleted of globin transcripts using GlobinClear (Ambion). cDNA libraries were prepared from poly(A)$^+$ mRNA from *Nprl3* extended knockout and wild-type cultured foetal liver cells using the mRNA-Seq pair-end kit (Illumina) and then sequenced using massively parallel sequencing (Illumina, GAII) with 50-bp end reads. A total of 67 and 37 million reads were generated from *Nprl3* extended knockout ($\Delta P6\text{-}R3^{-/-}$) and wild type, respectively. Reads were mapped to the mm9 mouse genome build using TopHat 1.1.1b (Trapnell et al. 2009). Transcript abundances and differential expression were tested using Cufflinks and Cuffdiff (Mortazavi et al. 2008) with current Ensembl transcript ID and Refseq gene

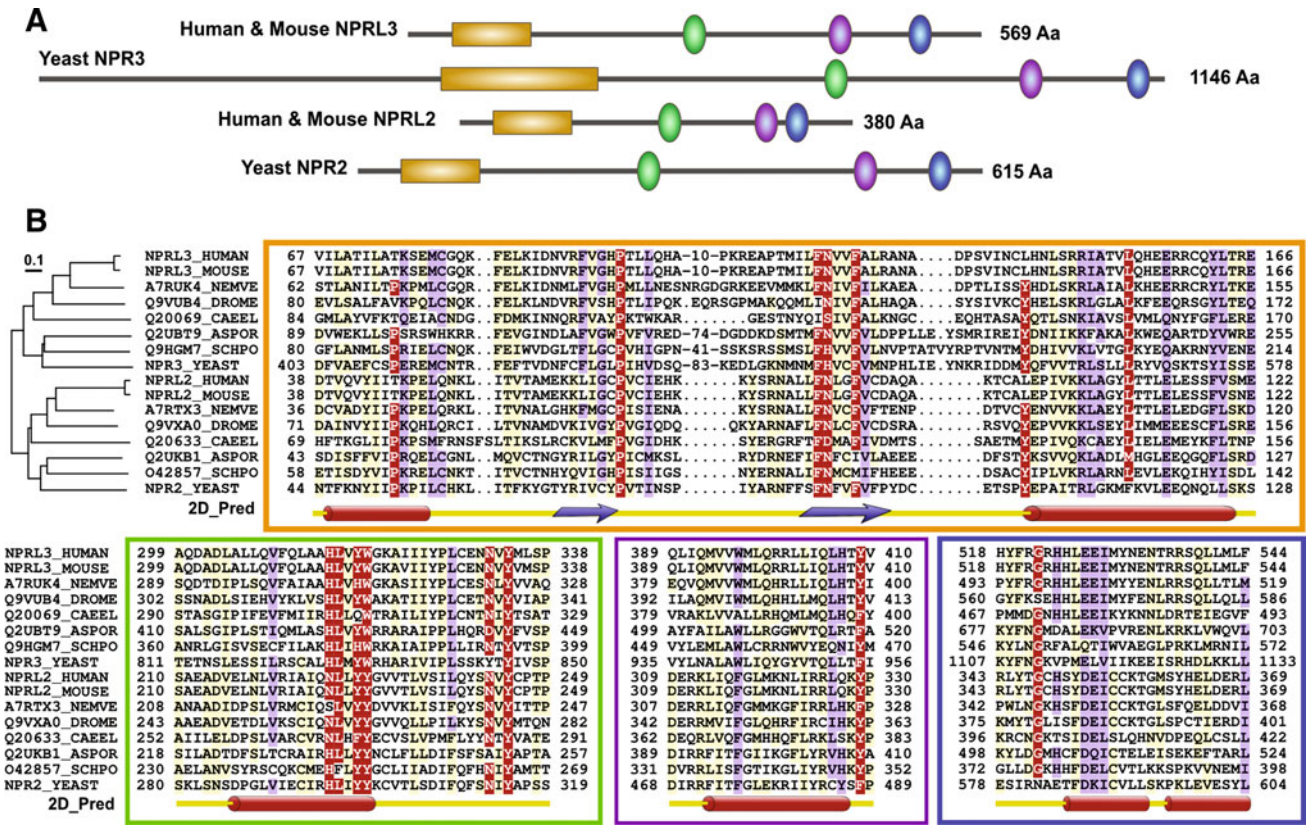

Fig. 1 Conserved regions and architecture of the NPR2 and NPR3 family. **a** Schematic representation of evolutionarily conserved regions present in both NPR2 and NPR3 families. The NPR3 family is represented by distantly related orthologous proteins, human and mouse NPRL3, and yeast Npr3. Similarly, the NPR2 family is represented by human and mouse NPRL2 and yeast Npr2. NPRL3 and Npr3 in turn are paralogues of human NPRL2 and yeast Npr2. Conserved regions between the two families are colour-coded. The most conserved region (shown in *orange*) is present at the N termini of the proteins, which show no similarity to any known domains. The protein's C-terminal region contains three consecutive helix-turn-helix (HTH) domains shown in *green*, *purple*, and *blue*. Protein names and lengths in amino acids are provided for each protein schematic. **b** Representative multiple sequence alignments of the N-terminal conserved domain (*orange box*) and the most conserved regions of three consecutive HTH domains (*green*, *purple*, and *blue boxes*). Sequences are named according to UniProt with the following species abbreviations: HUMAN, *Homo sapiens*; MOUSE, *Mus musculus*; NEMVE, *Nematostella vectensis*; DROME, *Drosophila melanogaster*; CAEEL, *Caenorhabditis elegans*; ASPOR, *Aspergillus oryzae*; SCHPO, *Schizosaccharomyces pombe*; YEAST, *Saccharomyces cerevisiae*. The amino acid colouring scheme indicates average BLOSUM62 scores (which are correlated with amino acid conservation) for each alignment column: red (greater than 3), violet (between 3 and 1.5), and light yellow (between 1.5 and 0.5). Numbers within the alignment represent sequences that have been excised. The tree indicates phyletically representative members of both families (NPR3 and NPR2). The *scale bar* represents an average number of amino acid substitutions per site (0.1). Secondary structure predictions were performed using PsiPred (46) and are shown below the alignments. Alpha helices and beta strands are indicated by *red cylinders* and *violet arrows*, respectively (Color figure online)

annotation. Gene ontology analysis was performed using DAVID (da Huang et al. 2009). RNA-Seq data has been submitted to NCBI Gene Expression Omnibus (GSE26877).

Animal work

All animal work was carried out according to UK Home Office regulations under the appropriate project licenses. Mice were killed by cervical dislocation and dissections performed immediately. To obtain staged mouse embryos, the morning on which a vaginal plug was noted was taken as embryonic day 0.5. Embryos were dissected from the uterus and placenta as described in Nagy et al. (2003).

Histology

Embryos were fixed overnight at 4 °C in 4 % PFA, washed twice in PBT (PBS + 0.1 % Tween 20), and dehydrated by sequential washing in 25, 50, and 75 % ethanol in PBT and finally by two washes in 100 % ethanol. For embedding in paraffin wax, embryos were washed twice in Histoclear II (National Diagnostics) and immersed in Paraplast compound (Sigma) at 60 °C for 3–6 h prior to embedding. Six-micron sections were cut and mounted on Superfrost® Plus microscope slides (VWR International). Tissue sections were deparaffinised by incubation in Histoclear II for 8 min, rehydrated by sequential washing in 100, 95, and 70 % ethanol, stained with Ehrlich's hematoxylin (RA

Lamb) for 1 min, and washed with tap water for 2 min. Sections were stained with 0.1 % eosin (RA Lamb) for 1 min. Stained sections were washed in tap water for 2 min, hydrated in ascending ethanol solutions (70, 95, and twice in 100 %), washed twice in Histoclear II, and allowed to dry for 10 min. Subsequently, stained sections were mounted using glass coverslips (BDH) and Histomount (RA Lamb). Tissue sections were examined using a Leica light microscope and photographs taken using OpenLab software (Improvision).

Skeletal preps

Embryos for skeletal staining were dissected as described above and fixed in 95 % ethanol for 1–3 days. They were immersed in Alcian blue stain (Sigma) (75 % ethanol, 20 % acetic acid, 3 mg/ml Alcian blue) for 21–28 days at 37 °C. They were differentiated in 95 % ethanol, macerated in 1 % KOH for 1–5 days, and stained in 0.1 % aqueous Alizarin red (Sigma) for 24 h. Embryos were washed in tap water and cleared in 0.8 % KOH and 20 % glycerol, sequentially dehydrated, and stored in 50 % ethanol/50 % glycerol.

Magnetic resonance imaging

Single- and multiembryo imaging and data reconstruction and analysis were performed as described previously (Szumska et al. 2008).

Patients

DNA from 67 patients with dilated cardiomyopathy and/or left ventricular noncompaction and ventriculoseptal defects (VSD) that was collected in the Department of Cardiology of Children's Hospital Boston and the Department of Cardiovascular Medicine at the University of Oxford and that of 37 normal controls was used to survey the coding regions of the *Nprl3* gene. Patients from the UK were ascertained through the Department for Cardiovascular Medicine clinical practice or the practice of referring physicians and evaluated by physical examination, echocardiography, and/or cardiac MRI and ECG, allowing the diagnosis of Left Ventricular Non Compaction (LVNC) to be made. All participants gave informed consent and local research ethical approval (ref. 09/H0605/3) was obtained. Patients from US were ascertained at Children's Hospital Boston. The diagnoses were made on the basis of echocardiographic images interpreted by board-certified cardiologists. DNA samples and phenotypic information were collected under research projects approved by the Internal Review Board of Children's Hospital Boston with informed consent.

Sequencing

Amplicons over the coding regions of the human *NPRL3* gene were amplified with FastTaq (Roche). Sequencing was performed using Big Dye chemistry on Applied Biosystems PRISM 3730 Genetic Analyzer. All sequences were analysed using Mutation Surveyor software (SoftGenetics LCC).

Results

Computational sequence analysis of the NPRL3 family

Consistent with previous reports (Jordan et al. 2007; Lunardi et al. 2009; Neklesa and Davis 2009), we identified NPRL3 as a likely orthologue of yeast Npr3. Sequence similarity between yeast Npr3 and human NPRL3 proteins was statistically highly significant ($E < 10^{-5}$). Moreover, database searches using Npr3 also identified it to be a remote homologue of a second family of proteins (Fig. 1a, b), namely, the NPR2 family (Pfam family: NPR2). Iterative interrogation of protein sequence databases using HMMer, a profile-to-sequence comparison method (Eddy 1996), with the N-terminal region of human NPRL3 (UniProt:Q12980; amino acids 66–168) as the query, identified remote homologues in the NPR2 family (Fig. 1a, b) with statistically significant E values (inclusion threshold $E < 0.005$). A similar, but reciprocal, search using human NPRL2 (UniProt:Q8WTW4; amino acids 37–124) as the query corroborated the evolutionary relationship of Npr3 and Npr2 families. Consequently, members of the NPR2 and NPR3 families are also homologous and thus share a common ancient ancestry. These results are in agreement with those recently generated automatically by PFAM (Clan:NPR/CL0435) (Finn et al. 2010).

Multiple alignment of NPR2 and NPR3 sequences reveals evolutionarily conserved regions shared between both families (Fig. 1b). The proteins' N-terminal regions contain the most conserved sequence between these families (shown in orange in Fig. 1a), whilst their C-terminal regions contain three homologous sequences (green, purple, and blue ovals in Fig. 1a) present in all NPR2 and NPR3 protein family members. A protein domain hunting strategy, based on profile–profile comparisons and protein structure prediction using HHpred (Soding et al. 2005), demonstrated that these regions contain consecutive helix-turn-helix domains (indicated in green, purple, and blue in Fig. 1a, b; HHpred probability >94 %; $E = 0.021$) that point to their potential roles in binding nucleic acid (RNA or DNA) rather than protein molecules (Aravind et al. 2005; Yoshizawa et al. 2005), although we do not rule out the latter. These sequence similarities were all highly

significant, thereby indicating homologies (Supplementary Fig. 1). Sequence conservation between the two families is illustrated in Fig. 1b.

These findings therefore show that not only is human NPRL3 a yeast Npr3 orthologue, it is also a paralogue of NPRL2, with which it heterodimerises (Neklesa and Davis 2009). Yeast Npr2 and Npr3 are known to bind proteins in common, including Cdc45 (Tong et al. 2004), Csm3 (Pan et al. 2006), and Hsp82 (McClellan et al. 2007). These observations are consistent with Npr2 and Npr3 being subunits of a heterodimer, since paralogues often possess common interaction partners (Baudot et al. 2004; Musso et al. 2007).

Transcriptome analysis

We previously generated two mouse models in which the *Nprl3* promoter sequence was deleted by homologous recombination ($\Delta P6^{-/-}$ and $\Delta P6\text{-}R3^{-/-}$) (Kowalczyk et al., 2012) (see schematic diagram in Supplementary Fig. 2). Both models abolished *Nprl3* transcription in all tissues tested apart from erythroid cells. We have recently shown that transcription of *Nprl3*-related RNAs in erythroid cells originates from intragenic, erythroid-specific enhancers embedded in the *Nprl3* gene which produce noncoding RNAs (so-called meRNAs). Importantly, the subtle 2.3-kb promoter deletion ($\Delta P6$) abolished expression of the *Nprl3*-encoded protein in all tissues (Kowalczyk et al. 2012).

To assess the general consequences of *Nprl3* inactivation, we next analysed the transcriptomes of erythroid cells derived from either wild-type or homozygous mutant ($\Delta P6\text{-}R3^{-/-}$) mice previously generated by our laboratory (Kowalczyk et al. 2012). Although either mouse model could have been analysed for this purpose, we chose to analyse $\Delta P6\text{-}R3^{-/-}$ mice. As expected, in the absence of the promoter, we observed only multiexonic RNA transcripts (meRNAs) originating from the remaining intragenic enhancers within the *Nprl3* locus. Since these meRNA transcripts have low coding potential, as expected, no NPRL3-associated protein was detected (Kowalczyk et al. 2012).

RNA transcripts from wild-type and mutant ($\Delta P6\text{-}R3^{-/-}$) cells were assembled and gene expression levels inferred (as FPKM values: fragments per kilobase of exon model per million mapped fragments) using TopHat and Cufflinks (Trapnell et al. 2009, 2010) and current RefSeq and Ensembl gene models, including mitochondrial genome genes. Considering only expressed genes (FPKM >10) in either mutant or wild-type samples, 4,513 significantly differentially expressed genes were identified using Cuffdiff (Trapnell et al. 2010). To investigate whether these differentially expressed genes are randomly distributed throughout Gene Ontology (GO) annotations (Gene Ontology Consortium 2010), we used DAVID (da Huang et al. 2009) to apply the one-tail Fisher's exact test followed by Benjamini's false discovery rate correction on the full set of GO terms.

The transcriptome of $\Delta P6\text{-}R3^{-/-}$ mice differed substantially from that of wild-type mice, with 101 and 51 GO terms being significantly ($p < 0.1$) enriched among genes up- and downregulated, respectively, in the mutant mice. The most significant annotation cluster enriched in upregulated genes contained five GO terms related to ribosomal biogenesis (Table 1). The most significant annotation cluster enriched in downregulated genes contained ten GO terms related to cell cycle (Table 1). A more stringent analysis identified the most significantly enriched GO terms that were consistent with the cluster analysis and further confirmed involvement in ribosomal biogenesis and cell cycle (Supplementary Table 1). These findings are consistent with a role for Nprl3 in regulating the well-documented pathway by which mTOR controls ribosomal biogenesis, protein synthesis, and the cell cycle (Wang and Proud 2006). This analysis was performed in erythroid cells, and, therefore, given the widespread pattern of Nprl3 expression, it will be important in the future to examine other cell types.

Phenotype of *Nprl3* mutant

Male and female $\Delta P6^{+/-}$ mice grew and bred normally indicating that loss of one functional allele resulted in no major detectable phenotypic effects. $\Delta P6^{+/-} \times \Delta P6^{+/-}$ matings resulted in variable-sized litters. Genomic analysis of tail DNA taken at day 14 after birth revealed no $\Delta P6^{-/-}$ mice among 128 weaned offspring of these intercrosses (Table 2). Both WT and heterozygote offspring were born with the expected Mendelian ratio (χ^2 test, $p = 0.059$). This indicated either embryonic or perinatal lethality of $\Delta P6^{-/-}$ mice.

To determine the developmental stage at which $\Delta P6^{-/-}$ embryos were lost, embryos from timed matings of $\Delta P6^{+/-}$ were retrieved on various days post-coitum (dpc). In total, 175 embryos between 10.5 and 15.5 dpc were examined and as a cohort the expected Mendelian distribution for all three genotypes (WT, $\Delta P6^{+/-}$, and $\Delta P6^{-/-}$) was observed (Table 2). Most of the $\Delta P6^{-/-}$ embryos were found dead prior to delivery (18.5 dpc). These results suggest that mutant mice die between 15.5 dpc and birth.

To determine the causes of this embryonic and/or perinatal lethality, embryos derived at various time points of development were examined to detect gross phenotypic abnormalities. Embryos were inspected in detail at four different stages of mid- to late gestation (10.5, 12.5, 14.5, and 15.5 dpc). $\Delta P6^{-/-}$ embryos from 10.5 dpc appeared

Table 1 RNA sequencing results from ΔP6-R3

Cluster of GO terms significantly enriched in upregulated genes					
Annotation cluster 1	Enrichment score: 51.0				
GO term	Number of genes	*p* value	Fold enrichment	Benjamini	FDR
GO:0030529: ribonucleoprotein complex	177	3.63E-70	4.3	1.82E-67	5.23E-67
GO:0005840: ribosome	100	7.31E-54	5.9	1.84E-51	1.05E-50
GO:0003735: structural constituent of ribosome	87	2.90E-51	6.5	3.06E-48	4.61E-48
GO:0006412: translation	128	1.77E-50	4.4	5.31E-47	3.18E-47
GO:0005198: structural molecule activity	104	3.98E-20	2.6	1.05E-17	6.33E-17
Cluster of GO terms significantly enriched in downregulated genes					
Annotation cluster 1	Enrichment score: 41.4				
GO term	Number of genes	*p* value	Fold enrichment	Benjamini	FDR
GO:0007049: cell cycle	203	3.01E-60	3.4	8.72E-57	5.40E-57
GO:0000278: mitotic cell cycle	105	2.54E-42	4.4	3.67E-39	4.55E-39
GO:0051301: cell division	112	2.76E-41	4.1	2.66E-38	4.95E-38
GO:0022402: cell cycle process	133	6.30E-40	3.5	4.56E-37	1.13E-36
GO:0000087: M phase of mitotic cell cycle	90	1.94E-39	4.8	1.12E-36	3.48E-36
GO:0022403: cell cycle phase	119	4.49E-39	3.7	2.17E-36	8.06E-36
GO:0000280: nuclear division	86	1.14E-36	4.6	4.70E-34	2.04E-33
GO:0007067: mitosis	86	1.14E-36	4.6	4.70E-34	2.04E-33
GO:0048285: organelle fission	87	4.33E-36	4.5	1.57E-33	7.76E-33
GO:0000279: M phase	105	1.93E-35	3.8	6.22E-33	3.47E-32

The results of Gene Ontology cluster analysis performed using DAVID. The first most significant clusters with highest enrichment scores and their components (GO terms) are presented. The number of genes representing each of the GO terms with associated *p* value is given

FDR false discovery rate

Table 2 Crosses were carried out between $\Delta P6^{+/-}$

Genotype	Wild type $\Delta P6^{+/+}$	Heterozygote $\Delta P6^{+/-}$	Homozygote $\Delta P6^{-/-}$	Total –
Expected mendelian %	25	50	25	100
After birth (%)	52 (41)	76 (59)	–	128 (100)
10.5 dpc (No. observed)	8	24	8	40
12.5 dpc (No. observed)	8	18	7	33
14.5 dpc (No. observed)	11	25	17	53
15.5 dpc (No. observed)	12	24	13	49
Total	39 (22 %)	91 (52 %)	45 (26 %)	175 (100 %)

Litters were genotyped by PCR at the time indicated

normal and similar to the WT and $\Delta P6^{+/-}$ littermates. In general, $\Delta P6^{-/-}$ embryos could be morphologically distinguished from their WT littermates as early as 12.5 dpc and defects became more obvious at late gestation. The $\Delta P6^{-/-}$ embryos dissected at 15.5 dpc appeared slightly smaller and pale in comparison with their normal littermates.

Gross examination also showed that many $\Delta P6^{-/-}$ embryos had some defect of body wall closure producing small to large forms of umbilical hernia (liver hernia, Fig. 2a–f). In some embryos there was a complete failure to close the ventral body wall and thoracic cavity (Supplementary Fig. 3a, b). In the latter case, abdominal and thoracic organs (heart and intestines) were exposed through an open rib cage. At 15.5 dpc, it was rare that $\Delta P6^{-/-}$ embryos *in utero* were already dead as judged by the absence of heartbeat.

Most $\Delta P6^{-/-}$ embryos had hemorrhages and fragmented vasculature. Generalised oedema was frequently seen and in some cases nuchal translucency was also present (Fig. 2f). The development of such oedema is frequently associated with cardiovascular defects (Haak et al. 2002).

The *Nprl3* knockout exerts a major effect on cardiovascular development

To determine the cause of perinatal lethality in more detail, we examined the structure of the internal organs of $\Delta P6^{-/-}$ mice. Two such embryos were sectioned (coronally and sagitally) and their tissues stained with hematoxylin and eosin (H&E). The histological examination and comparison of $\Delta P6^{-/-}$ and WT littermates showed that most major internal organs were present and generally of similar, normal appearance.

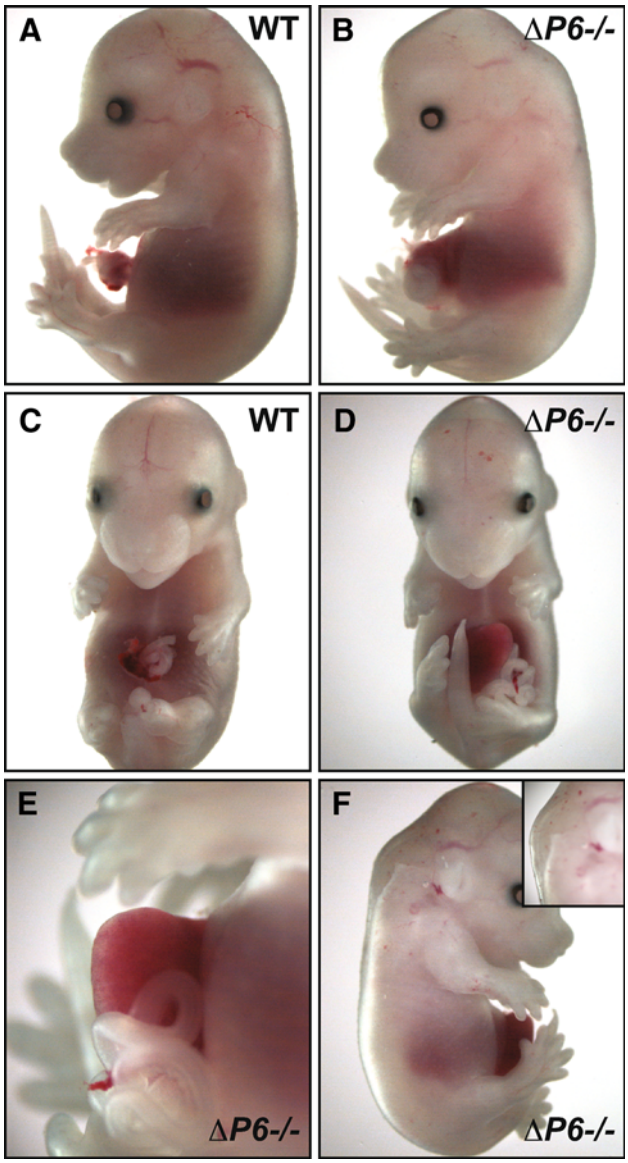

Fig. 2 Phenotypic abnormalities in $\Delta P6^{-/-}$ mutant mice. **a–f** Phenotypic abnormalities at 15.5 dpc of WT (**a**, **c**) and $\Delta P6^{-/-}$ (**b**, **d–f**) embryos. At 15.5 dpc in WT, withdrawal of the midgut hernia is almost complete, as shown from *side view* (**a**) and *ventral view* (**c**). In contrast, $\Delta P6^{-/-}$ mice show a large midline defect of the ventral body wall through which not only the midgut but also the liver can be seen to be herniated (**b**, **d**). **e** Higher magnification of the liver hernia. **f** Generalised oedema seen along the body; prominent nuchal translucency is shown in the *enlarged inset*

The major abnormalities in mutant homozygote embryos were detected in the heart and great vessels. By this stage of development, WT hearts are four-chambered (Fig. 3a, b) and all major structures are fully developed. The ventricular muscle is dense and the trabeculi are organised on the inner side of the thick compact zone (Fig. 3a, b). By contrast, hearts of $\Delta P6^{-/-}$ embryos were dramatically enlarged (Fig. 3c, d) compared to those of WT littermates (Fig. 3a, b). *Nprl3*-deficient hearts contained all four chambers (Fig. 3c, d), separated as expected and with mitral and tricuspid valves. However, the ventricles were dilated and abnormally structured (Fig. 3c, d). Detailed analysis showed prominent clear passage between the ventricles (ventricular septal defect, VSD) in both $\Delta P6^{-/-}$ embryos initially examined (Fig. 3d). Moreover, in *Nprl3*-deficient hearts the ventricles were severely hypoplastic and their compact muscle layer was almost absent (Fig. 3c, d). The trabeculi of the left ventricle were hypertrophic with deep intertrabecular recesses (Fig. 3c, d). The myocardium of the right ventricle was similarly disorganised (Fig. 3c, d). This demonstrates that *Nprl3*-deficient hearts have disrupted condensation of the myocardium.

In addition to these studies we examined several $\Delta P6^{-/-}$ embryos using magnetic resonance imaging (MRI), which was previously reported to allow identification of congenital malformations with high spatial resolution (Schneider et al. 2004) and which had been used to analyse subtle cardiac and visceral malformations in late gestation mouse embryos (Szumska et al. 2008). Analysis was performed on 10 $\Delta P6^{-/-}$ embryos, 14 $\Delta P6^{+/-}$ embryos, and 8 WT embryos from $\Delta P6^{+/-}$ intercrosses retrieved at 14.5 and 15.5 dpc. While there was no evidence of cardiac abnormalities in WT (Fig. 4a, b) or $\Delta P6^{+/-}$, $\Delta P6^{-/-}$ mice showed severe cardiac malformations, including ventricular septal defects, right-sided aortic arch and pulmonary artery (Fig. 4c, d), a right-sided pulmonary artery forming a vascular ring with normally localised aortic arch, and an interrupted aortic arch. Moreover, in one case there was a double-outlet right ventricle (DORV) or a form of overriding aorta, where the aorta is positioned directly over a VSD and not over the left ventricle. In three other $\Delta P6^{-/-}$ embryos the hearts were contracted precluding further analysis. The details of MRI-based malformations in $\Delta P6^{-/-}$ mice are summarised in Table 3.

In addition to these multiple cardiac malformations, there were other signs consistent with failure of blood perfusion and/or general heart failure, including general oedema together with pericardial oedema (Fig. 5a), dilated hepatic veins (data not shown), and large bilateral cysts in jugular lymphatic sacs (Fig. 5b). Additionally, in a subset

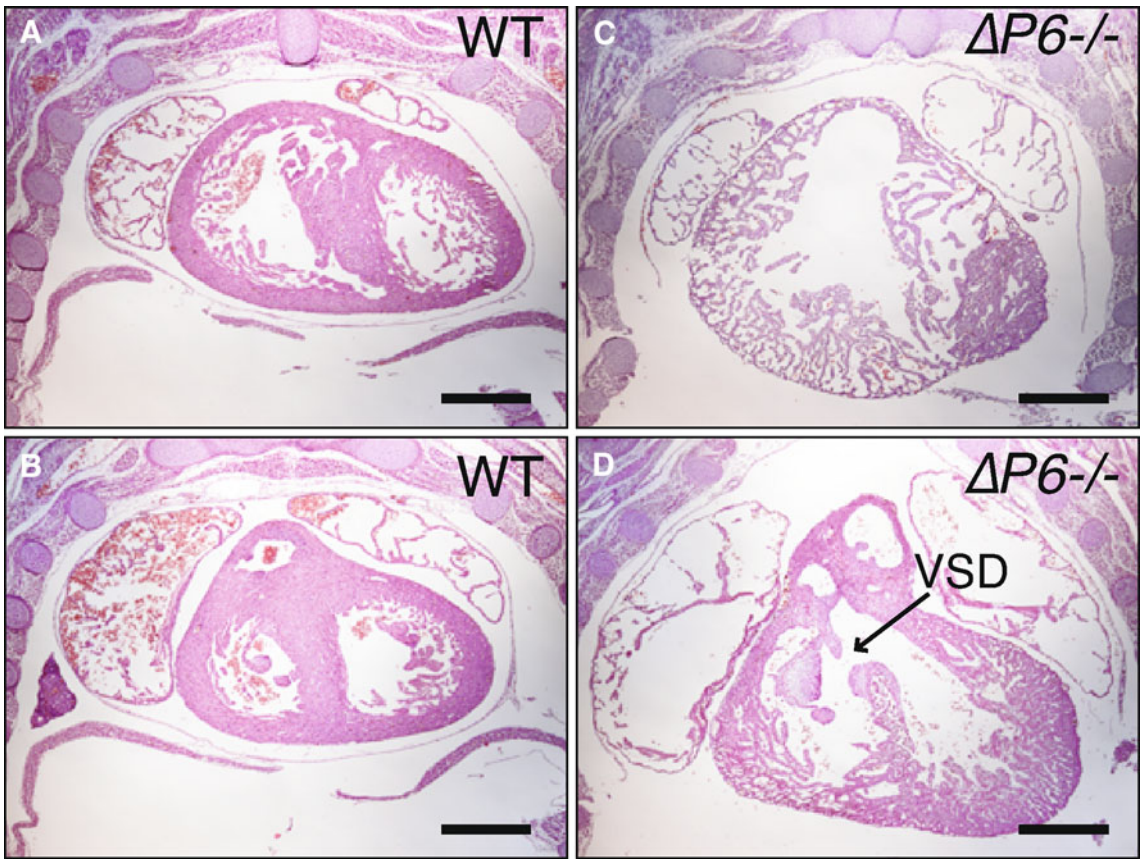

Fig. 3 Histological analysis of $\Delta P6^{-/-}$ hearts. The 15.5-dpc WT (**a**, **b**) and $\Delta P6^{-/-}$ (**c**, **d**) embryos were fixed, wax embedded, coronally sectioned, and hematoxylin–eosin-stained. $\Delta P6^{-/-}$ hearts (**c**, **d**) present abnormal structure of the myocardium. Right and left ventricles do not have a proper compact zone as seen in WT hearts (**a**, **b**). Coronal sections at the level of both ventricles in WT (**a**) and $\Delta P6^{-/-}$ (**c**) littermate. Coronal sections at the level of four chambers in WT (**b**) and $\Delta P6^{-/-}$ (**d**) littermate. $\Delta P6^{-/-}$ heart has a clear passage between left and right ventricle, a ventricular septal defect (VSD) (**d**). *Scale bars* = 0.5 mm. The sections are 7 μm thick

of $\Delta P6^{-/-}$ embryos, some internal organs (e.g., lungs, thymus, kidneys, and adrenals) appeared to be smaller as judged by eye. Liver hernia was frequently seen. Similarly, cleft palate was observed (Fig. 5c, d). The body size of some *Nprl3*-deficient embryos was noted to be decreased.

Using the multiembryo MRI technique, a wider range of malformations was observed in $\Delta P6^{-/-}$ embryos at 14.5 dpc than was detected by standard histological analysis. Importantly, $\Delta P6^{+/-}$ mice did not show any of the features described in $\Delta P6^{-/-}$ mice except for one which had a large cleft palate. The remaining embryos did not differ significantly from WT littermates. Finally, we examined skeletal morphology which showed no abnormalities (data not shown).

In summary, these findings showed that mice in which the promoter of the *Nprl3* gene had been deleted died in late gestation, often with severe cardiac defects.

Analysis of individuals hemizygous for *NPRL3*

Although heterozygous mice appeared to survive normally, it was of interest to determine whether human heterozygotes, with long life spans and potential exposure to environmental stresses, display any evidence for abnormal myocardial structure or function or any other late-developing congenital abnormalities. Two previously reported individuals with α-thalassaemia due to deletions that also inactivate *NPRL3* (Hatton et al. 1990; Wilkie et al. 1990) were investigated. Neither had any symptoms or signs attributable to cardiac dysfunction and MRI scans of their hearts revealed no significant abnormalities (data not shown). Furthermore, we also investigated 12 patients previously diagnosed with left ventricular noncompaction (resembling the myocardial defect seen in $\Delta P6^{-/-}$ mice) to determine whether they had associated α-thalassaemia (due to removal of *NRPL3* gene and the *α-globin* regulatory elements) but found no such instance.

Finally, we performed a pilot study in a cohort of patients with various types of cardiomyopathy and/or left ventricular noncompaction and ventricular septal defects (VSD) to look for possible disease-causing mutations within the *NPRL3* gene. We screened coding regions of *NPRL3* in 67 patients and 37 normal controls by direct

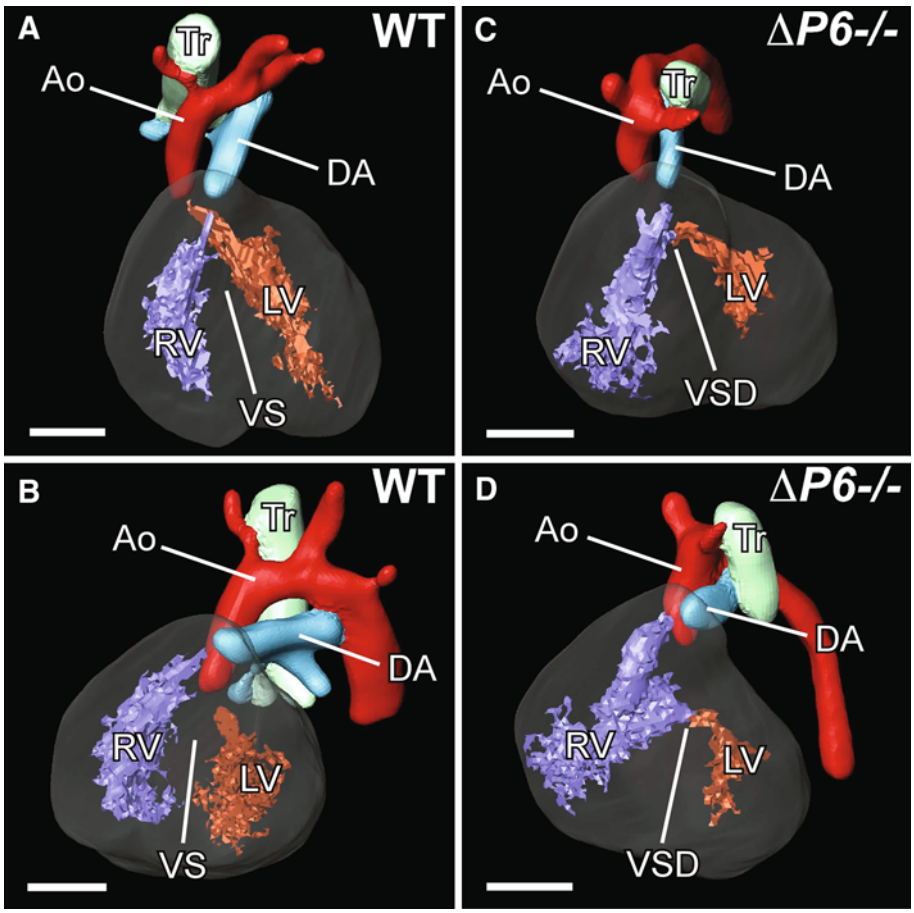

Fig. 4 Heart anomalies in $\Delta P6^{-/-}$ mutant mice by magnetic resonance imaging (MRI). 3D reconstructions of the heart from control (WT) (**a**, **b**) and $\Delta P6^{-/-}$ embryos (**c**, **d**), respectively. The $\Delta P6^{-/-}$ embryo (**c**, **d**) has a ventricular septal defect (VSD) and right-sided aortic arch and pulmonary artery (**c**, **d**). The right ventricle (RV) and left ventricle (LV), the trachea (Tr), aorta (Ao), and ductus arteriosus (DA) are indicated. The ventricular septum (VS) is indicated on the control embryo. Embryos were photographed at 14.5 dpc. *Scale bars* = 0.5 mm

sequencing. We identified three well-described single nucleotide polymorphisms (SNPs) and one polymorphism not found in current SNP databases (Table 4). Despite these searches no disease-causing mutations were found in the patients studied here.

Discussion

Evolutionary studies have shown that the prototypical globin cluster has been located adjacent to a widely expressed gene (*NPRL3*) in all species since the evolution of jawed vertebrates more than 450 million years ago (Hughes et al. 2005). Key *cis*-acting regulatory elements that control expression of the *α-globin* genes lie within the introns of this gene. This may account for the conserved synteny between *C16orf35* and the *α-globin* cluster. We previously noted that many deletions that cause α-thalassaemia in humans also inactivate *C16orf35*, and heterozygotes for such mutations appear to be phenotypically normal. The role of this highly conserved gene remained unknown.

Here we have confirmed that NPRL3 is the orthologue of the yeast protein Npr3 (nitrogen permease regulator 3) (Neklesa and Davis 2009), whose name originates from the observation that the yeast protein acts as part of a complex (with Npr2) which senses amino acid starvation. The Npr2/Npr3 complex influences cell metabolism via the mTOR pathway (Neklesa and Davis 2009). By separating the protein structure into smaller domains we were able to show for the first time that Npr3 and its interacting partner Npr2 are, in fact, paralogues, as are their human and mouse counterparts (NPRL3 and NPRL2). Although it has been shown that NPRL2 and NPRL3 physically interact with each other (Neklesa and Davis 2009), it remains to be seen whether, like their yeast orthologues, they act via the mTOR pathway. The wide phylogenetic distributions of NPR2 and NPR3 orthologues, which are highly conserved in sequence and domain architecture from yeast to human, certainly suggest that they perform fundamental cellular roles.

Of interest, we found that inactivation of the mouse *Nprl3* gene leads to a substantial increase in expression of many ribosomal protein genes and reduction of cell cycle-associated genes. Since disruption of yeast Npr2 or Npr3 is also known to result in a large (~2.5-fold) increase in ribosomal protein subunit gene expression and causes a severe proliferation defect (Neklesa and Davis 2009),

Table 3 The MRI-based malformations in $\Delta P6^{-/-}$ mouse embryos at 14.5 dpc

Phenotype	MP term	KO ($n = 6$)	Het ($n = 7$)	WT ($n = 5$)
Heart				
Left severe	MP:0006065	2	0	0
Pericardial oedema	MP:0001787	3	0	0
VSD	MP:0000281	4	0	0
DORV	MP:0000284	4	0	0
IAA	MP:0004157	1	0	0
R-sided AoA	MP:0004158	1	0	0
R-sided PA	MP:0000486	2	0	0
Other malformations				
Small embryo	MP:0001698	2	1	0
Large/medium oedema	MP:0001785	3	0	0
Large/medium cleft palate	MP:0000111	5	2	0
Small abnormal thymus	MP:0000706 MP:0002367	4	0	0
Cysts in jugular lymphatic sacks	MP:0004107	2	0	0
Small kidneys	MP:0002989	5	0	0
Small adrenal glands	MP:0002768	5	0	0
Small lungs	MP:0003641	4	0	0
Umbilical liver hernia	MP:0003052	3	0	0

Phenotypic data was annotated according to Mammalian Phenotype (MP) Ontology

DORV double outlet right ventricle, *VSD* ventricular septal defect, *IAA* interrupted aortic arch, *R-sided* right sided, *AoA* aortic arch, *PA* pulmonary artery

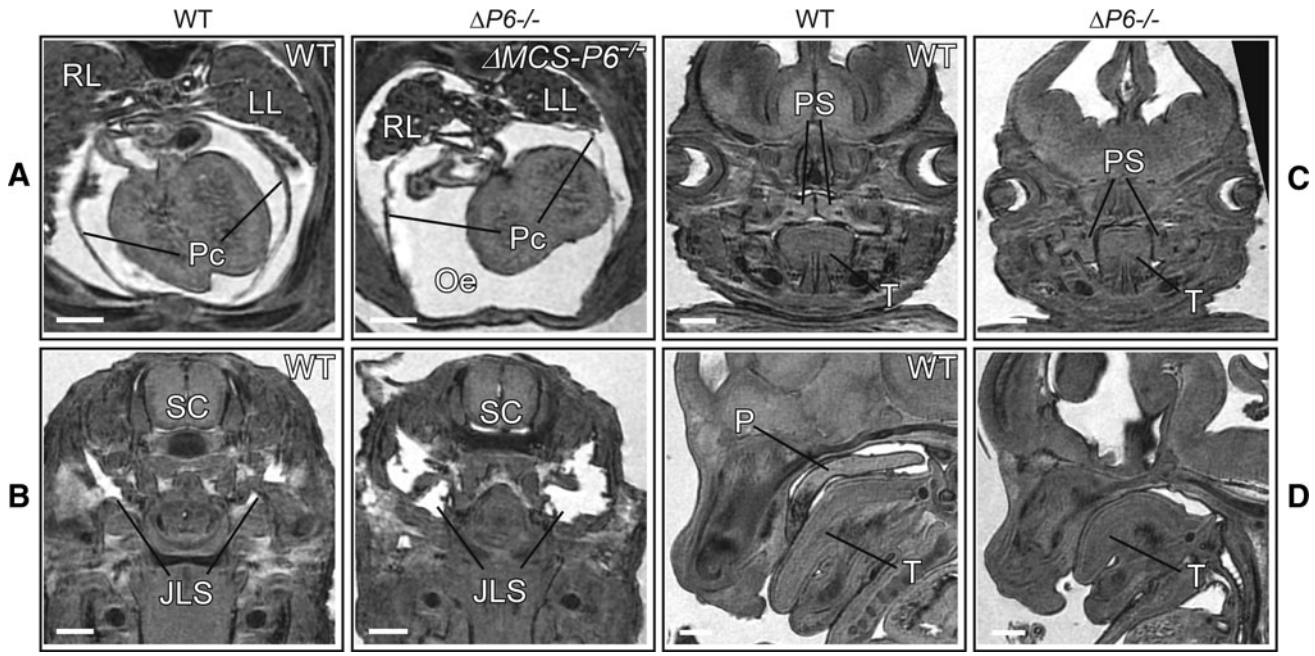

Fig. 5 Phenotypic anomalies in $\Delta P6^{-/-}$ mice shown by magnetic resonance imaging (MRI). MRI sections of $\Delta P6^{-/-}$ and control littermate (WT) embryos. Embryos were photographed at 14.5 dpc. **a** MRI transverse section through $\Delta P6^{-/-}$ and control embryos. The $\Delta P6^{-/-}$ embryo has marked pericardial oedema (Oe). Pericardium (Pc), right lung (RL), and left lung (LL) are indicated. **b** MRI section through $\Delta P6^{-/-}$ and control embryos. The $\Delta P6^{-/-}$ embryo has markedly enlarged jugular lymphatic sacs (JLS). Spinal cord (SC) is shown. **c** MRI coronal section through $\Delta P6^{-/-}$ and control embryos. The $\Delta P6^{-/-}$ embryo's palatal shelves are not fused compared to the WT littermate in which palatal shelves are completely fused by this stage of embryonic development. The tongue (T) and palatal shelves (PS) are indicated. **d** MRI sagittal section through $\Delta P6^{-/-}$ and control embryos. The $\Delta P6^{-/-}$ embryo lacks the palate (P). The tongue (T) is indicated. All *scale bars* = 0.5 mm

transcriptional coupling of Npr3, ribosomal protein genes, and cell cycle is clearly a conserved feature of both yeast and mammals. Yeast Npr2 and Npr3 act as regulators of the TOR complex 1 (TORC1), and loss of TOR results in inhibition of ribosomal protein gene transcription (Hardwick et al. 1999; Powers and Walter 1999). Consequently,

Table 4 The sequence analysis of coding regions of human *NPRL3* gene

Known SNP (dbSNP build 131)	Genome coordinates (hg19)	Type of change	Amino acid change (nucleotide change)	Known frequency (average hetorozygosity)	Number of samples with the change
rs11558704	Chr 16: 143224–143224	Nonsynonymous coding	V/L (G/GT)	NA	2
not found in dbSNP	Chr 16: 143302–143302	Synonymous coding	L/L (C/CT)	NA	1
rs1128426	Chr 16: 142714–142714	Synonymous coding	P/P (G/GA)	0.153 ± 0.23	11
rs58036849	Chr 16: 138755–138755	Nonsynonymous coding	A/T (G/GA)	NA	2

The table lists observed DNA changes among 104 DNA samples surveyed. SNPs were annotated according to SNP database (dbSNP, build 131). We also noticed that all the samples studied had an insertion, which is annotated as a SNP (rs57321480; rs71723243)

NA not applicable

it appears that both yeast Npr3 and mouse Nprl3 may act by suppressing TOR-dependent transcription of ribosomal protein genes and affect the cell cycle. Further investigation of mammalian Nprl3 may elucidate how it affects mTOR signaling and how this controls protein synthesis and the cell cycle.

Analysis of $\Delta P6^{-/-}$ embryos showed that the Nprl3 protein is essential for normal mouse development. Consistent with its widespread pattern of expression (Mitiku and Baker 2007), we noted a variety of developmental abnormalities affecting many different organs when the *Nprl3* gene is deleted. Nevertheless, the most consistent and dramatic effects are seen in heart development. These findings suggest that failure of normal cardiovascular development may, at least in part, be responsible for the observed embryonic/perinatal lethality. Although it is not known if NPRL2 and NPRL3 interact with the human mTOR pathway, it is interesting that mouse knockouts of the mTOR pathway components similarly lead to embryonic lethality (Guertin et al. 2006). Furthermore, in a wide range of studies (Shioi et al. 2002, 2003), including a conditional knockout model (Zhang et al. 2010), it has been shown that this pathway is important for the survival and normal function of cardiac cells.

Other malformations observed in $\Delta P6^{-/-}$ embryos, such as small internal organs and cleft palate, could be secondary to a compromised cardiovascular system, which may lead to insufficient blood flow to sustain rapid growth of developing embryos. Of course, given its ubiquitous pattern of expression, it is also possible that *Nprl3* may play a cell autonomous role in the proper development of other organs besides the heart. Again, these effects could be mediated by the mTOR pathway since many mutations of regulators lying upstream and downstream of this pathway have been associated with acquired and inherited genetic disorders in mice and humans (Inoki et al. 2005).

In summary, we have demonstrated that in a mouse model, disruption of *Nprl3* results in developmental defects (particularly in the cardiovascular system) leading to embryonic lethality late in gestation. Its wide conservation, widespread expression, and potential involvement in important general mechanisms and pathways suggest that NPRL3 underpins important cellular functions throughout development. Although the precise molecular functions of NPRL3 remain to be determined, the work presented here should focus future work on the normal role of NPRL3 and how mutations within it may give rise to human genetic disease.

Acknowledgments This work was supported by Marie Curie RTN EUrythron (MRTN-CT-2004-005499 to MSK), European Molecular Biology Organisation (ALT 325-2008 to LSP), Medical Research Council [Chris P. Ponting (C.P.P.) laboratory and Douglas R. Higgs (D.R.H.) laboratory], and the National Institute of Health Biomedical Research Centre Programme (D.R.H.) laboratory. We thank Dr. Taavi Neklesa for critically reading the manuscript. Thanks to Liz Ormondroyd from the Department of Cardiovascular Medicine (John Radcliffe Hospital, Oxford, UK) for collecting patients for the study. We also thank Pik-Shan Li, Christina Rode, and Sue Butler for assistance with transgenic lines production, breeding, and genotyping. We thank the patients for participation in this study.

Conflict of interest The authors have no conflicts of interests to declare.

References

Altschul SF, Madden TL, Schaffer AA, Zhang J, Zhang Z, Miller W, Lipman DJ (1997) Gapped BLAST and PSI-BLAST: a new generation of protein database search programs. Nucleic Acids Res 25:3389–3402

Aravind L, Anantharaman V, Balaji S, Babu MM, Iyer LM (2005) The many faces of the helix-turn-helix domain: transcription regulation and beyond. FEMS Microbiol Rev 29:231–262

Baudot A, Jacq B, Brun C (2004) A scale of functional divergence for yeast duplicated genes revealed from analysis of the protein–protein interaction network. Genome Biol 5:R76

da Huang W, Sherman BT, Lempicki RA (2009) Systematic and integrative analysis of large gene lists using DAVID bioinformatics resources. Nat Protoc 4:44–57

Dolznig H, Boulme F, Stangl K, Deiner EM, Mikulits W, Beug H, Mullner EW (2001) Establishment of normal, terminally differentiating mouse erythroid progenitors: molecular characterization by cDNA arrays. FASEB J 15:1442–1444

Eddy SR (1996) Hidden Markov models. Curr Opin Struct Biol 6:361–365

Finn RD, Mistry J, Tate J, Coggill P, Heger A, Pollington JE, Gavin OL, Gunasekaran P, Ceric G, Forslund K et al (2010) The Pfam protein families database. Nucleic Acids Res 38:D211–D222

Gene Ontology Consortium (2010) The gene ontology in 2010: extensions and refinements. Nucleic Acids Res 38:D331–D335

Guertin DA, Stevens DM, Thoreen CC, Burds AA, Kalaany NY, Moffat J, Brown M, Fitzgerald KJ, Sabatini DM (2006) Ablation in mice of the mTORC components raptor, rictor, or mLST8 reveals that mTORC2 is required for signaling to Akt-FOXO and PKCalpha, but not S6K1. Dev Cell 11:859–871

Haak MC, Bartelings MM, Jackson DG, Webb S, van Vugt JMG, Gittenberger-de Groot AC (2002) Increased nuchal translucency is associated with jugular lymphatic distension. Hum Reprod 17:1086–1092

Hardwick JS, Kuruvilla FG, Tong JK, Shamji AF, Schreiber SL (1999) Rapamycin-modulated transcription defines the subset of nutrient-sensitive signaling pathways directly controlled by the Tor proteins. Proc Natl Acad Sci USA 96:14866–14870

Hatton CS, Wilkie AO, Drysdale HC, Wood WG, Vickers MA, Sharpe J, Ayyub H, Pretorius IM, Buckle VJ, Higgs DR (1990) Alpha-thalassemia caused by a large (62 kb) deletion upstream of the human alpha globin gene cluster. Blood 76:221–227

Higgins DG, Thompson JD, Gibson TJ (1996) Using CLUSTAL for multiple sequence alignments. Methods Enzymol 266:383–402

Hughes JR, Cheng JF, Ventress N, Prabhakar S, Clark K, Anguita E, De Gobbi M, de Jong P, Rubin E, Higgs DR (2005) Annotation of cis-regulatory elements by identification, subclassification, and functional assessment of multispecies conserved sequences. Proc Natl Acad Sci USA 102:9830–9835

Inoki K, Corradetti MN, Guan KL (2005) Dysregulation of the TSC-mTOR pathway in human disease. Nat Genet 37:19–24

Jones DT (1999) Protein secondary structure prediction based on position-specific scoring matrices. J Mol Biol 292:195–202

Jordan PW, Klein F, Leach DR (2007) Novel roles for selected genes in meiotic DNA processing. PLoS Genet 3:e222

Kowalczyk MS, Hughes JR, Garrick D, Lynch MD, Sharpe JA, Sloane-Stanley JA, McGowan SJ, De Gobbi M, Hosseini M, Vernimmen D et al (2012) Intragenic enhancers act as alternative promoters. Mol Cell 45:447–458

Lower KM, Hughes JR, De Gobbi M, Henderson S, Viprakasit V, Fisher C, Goriely A, Ayyub H, Sloane-Stanley J, Vernimmen D et al (2009) Adventitious changes in long-range gene expression caused by polymorphic structural variation and promoter competition. Proc Natl Acad Sci USA 106:21771–21776

Lunardi A, Chiacchiera F, D'Este E, Carotti M, Dal Ferro M, Di Minin G, Del Sal G, Collavin L (2009) The evolutionary conserved gene *C16orf35* encodes a nucleo-cytoplasmic protein that interacts with p73. Biochem Biophys Res Commun 388:428–433

Maciukenas M (1994) Treetool 2.0.2

McClellan AJ, Xia Y, Deutschbauer AM, Davis RW, Gerstein M, Frydman J (2007) Diverse cellular functions of the Hsp90 molecular chaperone uncovered using systems approaches. Cell 131:121–135

Mitiku N, Baker JC (2007) Genomic analysis of gastrulation and organogenesis in the mouse. Dev Cell 13:897–907

Mortazavi A, Williams BA, McCue K, Schaeffer L, Wold B (2008) Mapping and quantifying mammalian transcriptomes by RNA-Seq. Nat Methods 5:621–628

Musso G, Zhang Z, Emili A (2007) Retention of protein complex membership by ancient duplicated gene products in budding yeast. Trends Genet 23:266–269

Nagy A, Gertsenstein M, Vintersten K, Behringer R (2003) Manipulating the mouse embryo: a laborartory manual, 3rd edn. Cold Spring Harbor Laboratory Press, Cold Spring Harbor

Neklesa TK, Davis RW (2009) A genome-wide screen for regulators of TORC1 in response to amino acid starvation reveals a conserved Npr2/3 complex. PLoS Genet 5:e1000515

Notredame C, Higgins DG, Heringa J (2000) T-Coffee: a novel method for fast and accurate multiple sequence alignment. J Mol Biol 302:205–217

Pan X, Ye P, Yuan DS, Wang X, Bader JS, Boeke JD (2006) A DNA integrity network in the yeast *Saccharomyces cerevisiae*. Cell 124:1069–1081

Powers T, Walter P (1999) Regulation of ribosome biogenesis by the rapamycin-sensitive TOR-signaling pathway in *Saccharomyces cerevisiae*. Mol Biol Cell 10:987–1000

Saitou N, Nei M (1987) The neighbor-joining method: a new method for reconstructing phylogenetic trees. Mol Biol Evol 4:406–425

Schneider JE, Bose J, Bamforth SD, Gruber AD, Broadbent C, Clarke K, Neubauer S, Lengeling A, Bhattacharya S (2004) Identification of cardiac malformations in mice lacking Ptdsr using a novel high-throughput magnetic resonance imaging technique. BMC Dev Biol 4:16

Shioi T, McMullen JR, Kang PM, Douglas PS, Obata T, Franke TF, Cantley LC, Izumo S (2002) Akt/protein kinase B promotes organ growth in transgenic mice. Mol Cell Biol 22:2799–2809

Shioi T, McMullen JR, Tarnavski O, Converso K, Sherwood MC, Manning WJ, Izumo S (2003) Rapamycin attenuates load-induced cardiac hypertrophy in mice. Circulation 107:1664–1670

Soding J, Biegert A, Lupas AN (2005) The HHpred interactive server for protein homology detection and structure prediction. Nucleic Acids Res 33:W244–W248

Sonnhammer EL, Hollich V (2005) Scoredist: a simple and robust protein sequence distance estimator. BMC Bioinform 6:108

Szumska D, Pieles G, Essalmani R, Bilski M, Mesnard D, Kaur K, Franklyn A, El Omari K, Jefferis J, Bentham J et al (2008) VACTERL/caudal regression/Currarino syndrome-like malformations in mice with mutation in the proprotein convertase Pcsk5. Genes Dev 22:1465–1477

Tong AH, Lesage G, Bader GD, Ding H, Xu H, Xin X, Young J, Berriz GF, Brost RL, Chang M et al (2004) Global mapping of the yeast genetic interaction network. Science 303:808–813

Trapnell C, Pachter L, Salzberg SL (2009) TopHat: discovering splice junctions with RNA-Seq. Bioinformatics 25:1105–1111

Trapnell C, Williams BA, Pertea G, Mortazavi A, Kwan G, van Baren MJ, Salzberg SL, Wold BJ, Pachter L (2010) Transcript assembly and quantification by RNA-Seq reveals unannotated transcripts and isoform switching during cell differentiation. Nat Biotechnol 28:511–515

Wang X, Proud CG (2006) The mTOR pathway in the control of protein synthesis. Physiology (Bethesda) 21:362–369

Wilkie AO, Lamb J, Harris PC, Finney RD, Higgs DR (1990) A truncated human chromosome 16 associated with alpha thalassaemia is stabilized by addition of telomeric repeat (TTAGGG)n. Nature 346:868–871

Wu CH, Apweiler R, Bairoch A, Natale DA, Barker WC, Boeckmann B, Ferro S, Gasteiger E, Huang H, Lopez R et al (2006) The Universal Protein Resource (UniProt): an expanding universe of protein information. Nucleic Acids Res 34:D187–D191

Yoshizawa S, Rasubala L, Ose T, Kohda D, Fourmy D, Maenaka K (2005) Structural basis for mRNA recognition by elongation factor SelB. Nat Struct Mol Biol 12:198–203

Zhang Y (2008) I-TASSER server for protein 3D structure prediction. BMC Bioinform 9:40

Zhang D, Contu R, Latronico MV, Zhang J, Rizzi R, Catalucci D, Miyamoto S, Huang K, Ceci M, Gu Y et al (2010) MTORC1 regulates cardiac function and myocyte survival through 4E-BP1 inhibition in mice. J Clin Invest 120:2805–2816